


RESEARCH ARTICLE

Open Access



Biophysical mapping of TREM2-ligand interactions reveals shared surfaces for engagement of multiple Alzheimer's disease ligands

Jessica A. Greven¹, Joshua R. Wydra¹, Rory A. Greer², Cynthia Zhi¹, David A. Price³, Jordyn D. Svoboda¹, Christopher L. M. Camitta¹, Mya Washington¹, Daisy W. Leung³, Yuhua Song², Jen Alexander-Brett^{1,4,5,9*} and Tom J. Brett^{1,4,6,7,8,9*} 

Abstract

TREM2 is a signaling receptor expressed on microglia that has emerged as an important drug target for Alzheimer's disease and other neurodegenerative diseases. While a number of TREM2 ligands have been identified, little is known regarding the structural details of how they engage. To better understand this, we created a protein library of 28 different TREM2 variants that could be used to map interactions with various ligands using biolayer interferometry. The variants are located in previously identified putative binding surfaces on TREM2 called the hydrophobic site, basic site, and site 2. We found that mutations to the hydrophobic site ablated binding to apoE4 and TDP-43. Competition binding experiments indicated that apoE4 and oA β 42 share overlapping binding sites on TREM2. In contrast, binding to C1q was disrupted most strongly by mutations to the basic site, including R46, with some mutations to the hydrophobic site also attenuating binding, thus suggesting a broader mediation of binding across the two sites. Supporting this, competition experiments indicated that C1q binding could be blocked by both apoE and oA β 42. TREM2 binding to IL-34 was mediated by the basic site at a surface centering on R76. Competition binding experiments validated the unique site for IL-34, showing little to no competition with either oA β 42 or apoE4. However, competition experiments between C1q and IL34 suggest that the ligands compete for binding at the basic site. Altogether, our results suggest that TREM2 utilizes the hydrophobic site (consisting of CDR1, CDR2, and CDR3) as a common site to engage multiple ligands, and uses distinct basic sites to engage others. Our findings imply that pharmaceutical strategies targeting these surfaces might be effective to modulate TREM2 functions.

Keywords TREM2, Microglia, IL-34, TDP-43, Complement C1q, apoE, Amyloid beta, Alzheimer's disease

*Correspondence:
Jen Alexander-Brett
jalexand@wustl.edu
Tom J. Brett
tbrett@wustl.edu

Full list of author information is available at the end of the article



© The Author(s) 2025. **Open Access** This article is licensed under a Creative Commons Attribution 4.0 International License, which permits use, sharing, adaptation, distribution and reproduction in any medium or format, as long as you give appropriate credit to the original author(s) and the source, provide a link to the Creative Commons licence, and indicate if changes were made. The images or other third party material in this article are included in the article's Creative Commons licence, unless indicated otherwise in a credit line to the material. If material is not included in the article's Creative Commons licence and your intended use is not permitted by statutory regulation or exceeds the permitted use, you will need to obtain permission directly from the copyright holder. To view a copy of this licence, visit <http://creativecommons.org/licenses/by/4.0/>. The Creative Commons Public Domain Dedication waiver (<http://creativecommons.org/publicdomain/zero/1.0/>) applies to the data made available in this article, unless otherwise stated in a credit line to the data.

Introduction

The triggering receptor expressed on myeloid cells-2 (TREM2) plays a central role in regulating myeloid cell maturation and function in the setting of numerous human pathologies, including neurodegenerative diseases, metabolic diseases, and cancers [1]. The potential importance of TREM2 in neuronal health was first indicated by large-scale genetic studies that identified rare TREM2 point variants, namely R47H and R62H, as risk factors for developing late-onset Alzheimer's disease (AD) [2–4]. TREM2 is mainly expressed on macrophages and microglia and responds to ligands associated with tissue damage. Within the setting of neurodegenerative diseases, particularly AD, responses signaled through TREM2 trigger activation of microglia into a Damage Associated Microglia (DAM) phenotype. This signaling can enhance protective functions of microglia, including chemotaxis, phagocytosis, suppression of inflammatory signaling, and boosting microglia survival and proliferation [5]. In addition, TREM2 can be proteolytically released from the cell surface or alternatively spliced to produce soluble TREM2 (sTREM2), which also has beneficial functions in the setting of AD. For example, sTREM2 has been shown to reduce amyloid beta pathologies in AD mouse models [6], and increased sTREM2 levels in human CSF appear to correlate with increased cognitive reserve [7]. In addition, sTREM2 has been shown to bind amyloid beta (A β) and inhibit its aggregation [8, 9], and can also disaggregate A β oligomers and filaments [10]. For these and other reasons, TREM2 has emerged as a viable drug target for Alzheimer's disease, especially in the preclinical stage.

In recent years, a number of potential TREM2 ligands with relevance to AD have been identified. The first was apolipoprotein E (apoE) [11, 12], which also has an allelic variant, apoE4, that is a strong genetic risk factor for AD. ApoE has been shown to be a signaling ligand for TREM2 [13, 14] and its association with A β might assist the phagocytosis and degradation of A β oligomers by microglia via TREM2 [14]. Quite recently, oligomeric TDP-43 was also identified as a phagocytosis-triggering ligand for TREM2 [15]. TDP-43 is the main component of insoluble aggregates found in patients with ALS [16], and these aggregates have also been identified in FTD and AD [17]. Additionally, the cytokine IL-34 was recently identified as a TREM2 signaling ligand [18]. IL-34 has been linked to AD [19] and IL-34 mediated signaling in a microglial cell line was demonstrated [18]. The initial component of the complement system, C1q, was also recently shown to be a ligand for TREM2 [20]. However, instead of triggering signaling, C1q binding to TREM2 prevents activation of the complement pathway. The complement pathway is involved in pruning excess synapses during development, but these functions

become aberrantly activated in AD and contribute to synaptic loss and neurodegeneration [20]. TREM2 binding to C1q inhibits activation of the classical complement pathway and is protective against complement-mediated synaptic elimination. Although a number of functional ligands for TREM2 with distinct roles in AD pathogenesis have been identified, little is known regarding the structural mechanisms of their engagement. Such knowledge is critical not only to understand the structural basis for TREM2 functions, but is also crucial to design therapeutic strategies that target TREM2.

TREM2 is a single-pass transmembrane receptor consisting of an extracellular V-type Ig domain and intrinsically disordered stalk, transmembrane helix, and short cytoplasmic tail (Fig. 1A). This tail lacks any signal transduction or trafficking motifs, and TREM2 associates with the adaptor proteins DAP12 and DAP10 via transmembrane contacts to facilitate its trafficking and signaling. The Ig domain is likely the main region of TREM2 that engages extracellular ligands. We determined the first crystal structure of TREM2 and identified two potential ligand-binding surfaces on the Ig domain: a large hydrophobic site located on the distal end of the molecule in the CDR loops; and a large electropositive surface, termed the basic site, that stretches partly around the midsection of the protein ([21] and Fig. 1B). Since then, there have been few studies showing how these surfaces might be involved in binding ligands. A co-crystal structure of TREM2 in complex with a soluble analog of the phospholipid phosphatidylserine (PS) showed that the PS headgroup bound near the top of the basic site [22]. More recently, we showed that point mutations to the hydrophobic site diminished binding affinity for apoE4 almost 200-fold, suggesting that this protein mainly utilized the hydrophobic site on TREM2 for engagement [9]. In addition, a recent study used crosslinking and mass spectrometry to identify another region on TREM2 called site 2 that might engage oA β 42 [8].

In order to understand how TREM2 engages ligands of relevance to AD, we designed a panel of 28 different TREM2 variants that could be used in quantitative BLI binding assays to map TREM2 binding surfaces for various ligands. These mutations are mainly located in the previously identified binding surfaces in the hydrophobic site, basic site, and site 2. Here, we used this panel to map binding for the AD-relevant TREM2 ligands apoE, TDP-43, C1q, and IL-34. We found that apoE and TDP-43 bound at or near a common hydrophobic site, while C1q and IL-34 engage unique surfaces mainly located on the basic site. The results reveal an intriguing promiscuous binding surface on TREM2 and provide information to drive further functional and structural studies, as well as strategies for therapeutically targeting TREM2.

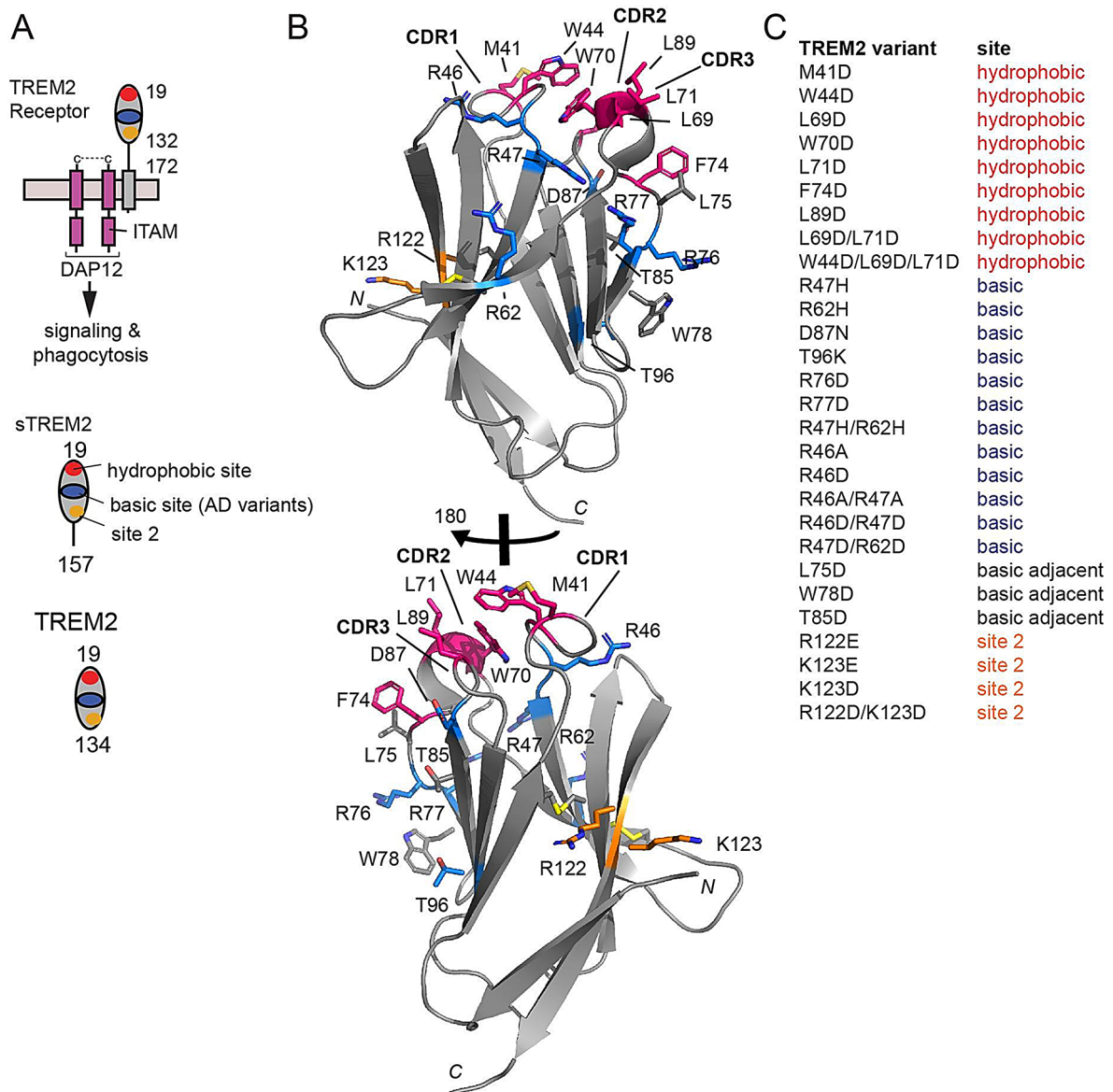


Fig. 1 Structure-guided TREM2 variants created to map interactions with ligands. **(A)** Schematic of TREM2 receptor on surface of microglia, and TREM2 versions described in this manuscript. **(B)** Ribbon diagram of TREM2 showing location of residues mutated, colored coded by site (red = hydrophobic; blue = basic; gray = basic adjacent; orange = site 2). **(C)** Table of all TREM2 variants produced for this manuscript or in our previous publications

Methods

Protein production and purification

TREM2 (19–134) and sTREM2 (19–157) variants were cloned into pHLsec vector using the Gibson assembly method. Constructs were verified by sequencing. For TREM2, these constructs were then excised by restriction digest (EcoRI-KpnI), gel purification, and ligation into pHLAvi to encode a C-terminal BirA biotinylation sequence. TREM2 WT and variants were produced in Expi293F cells, purified, and enzymatically biotinylated using BirA as described previously [9, 21]. ApoE4 was produced as reported previously [9]. Aβ42 was purchased from Anaspec. Oligomers were produced similar

to previous descriptions [23]. Briefly, peptides were first dissolved in hexafluoroisopropanol (HFIP) and allowed to air-dry overnight. They were then dissolved in DMSO at a concentration of 100 mM and sonicated for 10 min. These solutions were then diluted into PBS at a concentration of 22 μM and incubated at 37 °C for 3 h. Precise concentrations were then measured by BCA assay, after which the oAβ42 solutions were aliquoted, flash frozen, and stored at -80 °C. Freshly thawed aliquots were used for each experiment. Monomeric biotinylated oAβ42 was purchased from Anaspec and then mixed 1:20 with non-biotinylated monomeric Aβ42. These monomers were then oligomerized using the previously stated protocol.

oA β 42 preparations were characterized by negative stain transmission electron microscopy (TEM). Samples were prepared as previously mentioned and diluted to final A β 42 concentrations of 2.5 μ M. These TEM samples (10 μ l) were applied to carbonate-coated grids for 1 min and negatively stained with 1% phosphotungstic acid (PTA) for 1 min. TEM micrographs were obtained on a Hitachi H-7000 operated at 120 kV. Representative micrograph is shown in Supplemental Fig. 1. Human IL-34 (19–241) was cloned into pHLsec vector [24] and produced in Expi293F cells. The secreted IL-34 was purified from the media using NiNTA chromatography. Full length human TDP-43 was cloned into pET23b to contain a C-terminal 6-His tag. The protein was expressed in *E. coli* and purified from insoluble inclusion bodies. Purified TDP-43 was solubilized in a buffer with 6 M guanidine, 10 mM Tris pH 8.0, and 20 mM β -mercaptoethanol. Soluble TDP-43 oligomers were then made by 1:100 dilution into 100 mM Tris pH 8.5, 200 mM NaCl, 0.5 M arginine, and 750 mM guanidine. C1q protein was purchased from Complement Technology (Cat#A099). All proteins were analyzed by SDS-PAGE and found to be >95% pure. All proteins were immediately aliquoted, frozen, and stored at -80 °C for reproducible assays.

Binding studies by biolayer interferometry (BLI)

BLI data were collected on an Octet RED384 system (FortéBio). Biotinylated TREM2 were immobilized on streptavidin-coated (SA) biosensors and binding was measured using a running buffer of PBS with 0.1% BSA and 0.005% Tween-20. For experiments with immobilized TREM2 WT and variants, the following proteins were diluted into the running buffer in the following concentration ranges: apoE4 (0.012–50 μ M), TDP-43 (0.625–10 μ M), C1q (62.5–1000 nM), and IL-34 (62.5–1000 nM). Data were processed using double-reference subtraction (loaded protein into buffer and biotin-loaded pin into ligand) in FortéBio Data Analysis 9.0.

BLI competition binding experiments

BLI competition binding experiments were carried out as sequential binding experiments. Biotinylated TREM2 WT was immobilized on SA biosensors then dipped into wells containing either a first ligand or no ligand, then moved to buffer for dissociation, then moved to wells containing a second ligand. The ligand concentrations are listed in the figures and figure legends (Figs. 3, 6, and 9). The binding for the second ligand was quantitated as:

(Response at the end of Association 2) – (Response at the beginning of Association 2) and is shown in bar graphs in the appropriate figures (e.g., Figs. 2 and 3E and F).

TREM2-apoE4 binding ELISA assay

ELISA experiments were carried out essentially as described in [21]. In brief, apoE4 was diluted to 1 μ g/mL in PBS and 100 μ L/well was applied to high-absorption ELISA plates (NUNC, Thermo) and incubated at 25 °C for 12 h followed by wash 3x in wash buffer (PBS + 0.05% Tween 20). Wells were then blocked with reagent buffer (1% BSA in PBS) for 1 h at 25 °C. Biotinylated WT or mutant TREM2 were diluted in reagent buffer and incubated on ELISA plate for 1 h at 25 °C. Plates were washed 3x in wash buffer, then detection of bound biotinylated TREM2 was carried out by incubation with streptavidin-HRP (R&D Systems) in reagent buffer for 20 min at 25 °C before final 3x wash. Development was performed with TMB substrate (SeraCare). After quenching with 0.5 M HCl, absorbance was measured at 450 nm on a BioTek Synergy plate reader. Absorbance readings were plotted in Prism as mean \pm standard error of the mean and statistics were analyzed by One-way ANOVA. * p < 0.05, ** p < 0.01, *** p < 0.001.

Size exclusion chromatography-multiangle light scattering (SEC-MALS)

Ten (10) μ L of pure sTREM2 WT (2 mg/mL) was subjected to size-exclusion chromatography using a Superdex 200 Increase 5/150 GL column followed by UV, multi-angle light scattering, and refractive index detection using a Wyatt Technologies MALS configuration. Data analysis was performed using Wyatt Technologies ASTRA software.

Prediction of TREM2-IL-34 binding using computational methods

To identify residues on TREM2 and IL-34 that were likely to be involved with protein-protein interactions, we first ran the complete sequence of TREM2 and IL-34 (UniProt accession numbers Q9NZC2 and Q6ZMJ4, respectively) through PredictProtein [25] using ProNA2020 [26], which combines machine learning and homology-based inference to predict if the input sequence is a binding protein and then predict which residues are likely to participate in protein-protein interactions.

Next, we used an in-house hydropathy matching algorithm to predict likely binding sites between TREM2 and IL-34 [9]. We screened the six helices from IL-34 against the TREM2 immunoglobulin domain (residues 18–130). We then screened the three CDR loops that make up the hydrophobic site and the four strands that make up the basic site in TREM2 against the IL-34 sequence (excluding residues 1–20 which make up the signaling peptide). For each screening, the sequence was converted into binary (+ or -) hydrophobicity maps based on the hydrophobicity sign of each residue by the Kyte and Doolittle scale [27]. The hydrophobicity maps for each potential

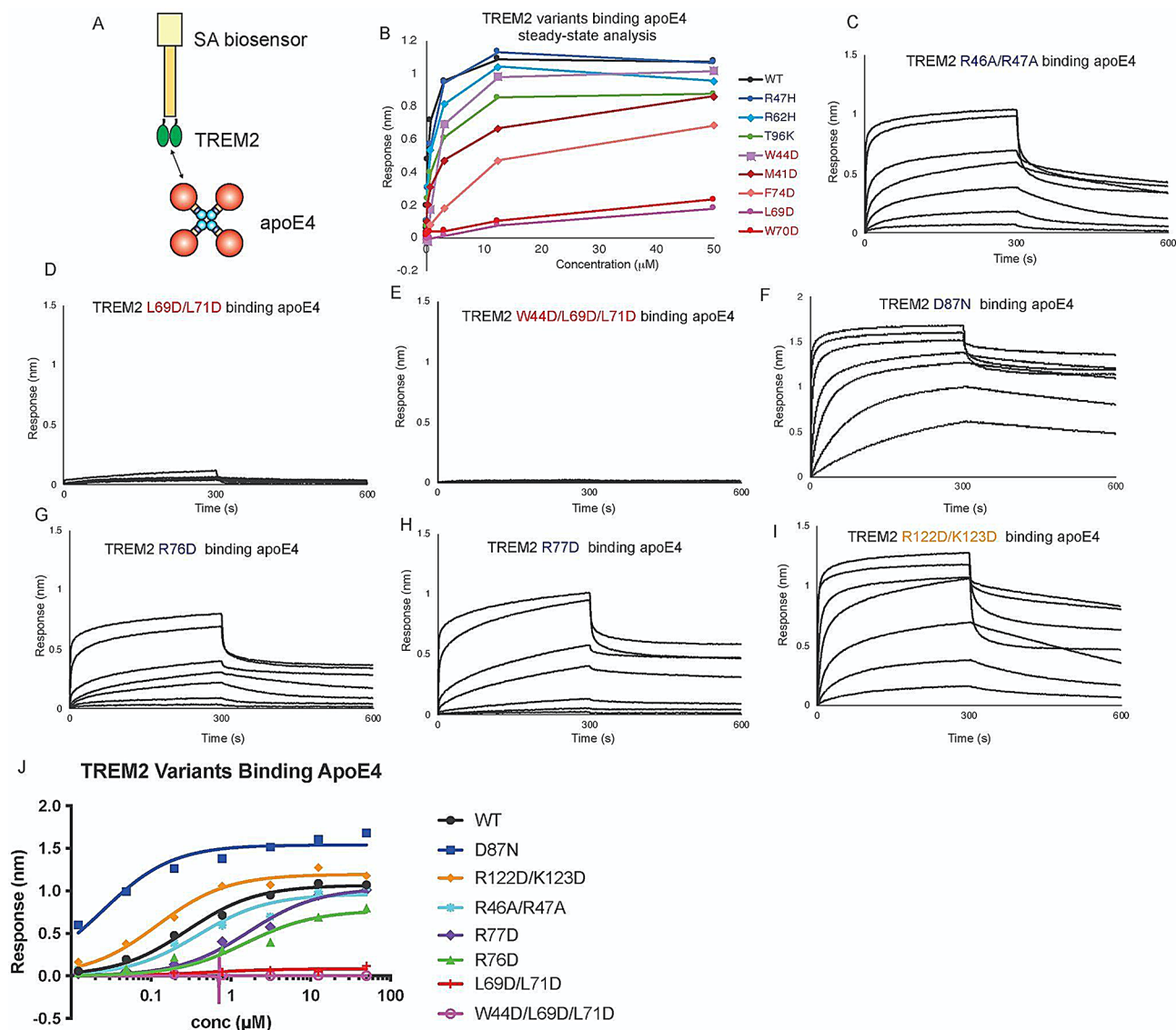


Fig. 2 Mutations to TREM2 hydrophobic site ablate binding to apoE4. Immobilized TREM2 WT and variants were probed for binding to apoE4 (0.012–50 μM). **(A)** Scheme of experiment. **(B)** Summary of steady-state binding for TREM2 WT and variants from our previous publication [9]. **(C–J)** BLI sensorgrams for TREM2 **(C)** R46A/R47A, **(D)** L69D/L71D, **(E)** W44D/L69D/L71D, **(F)** D87N, **(G)** R76D, **(H)** R77D, **(I)** R122D/K123D binding to apoE4 (0.012–50 μM). Double-reference subtracted data shown in black. **(J)** Steady state analysis and non-linear fits to derive K_D from data shown in **(C–I)**. The derived K_D s are listed in Table 1

binding motif were screened in both forward and reverse orientations against the entire hydrophobicity map of the other protein. The percent match was calculated as the percentage of dividing complementary (+/-) pairs to all matched pairs. The degree of complementary hydropathy (Eq. 1 [28]) was calculated based on the Kyte Doolittle hydropathy index [27].

$$C = \frac{\sum_{i=1}^L |H(i) - H'(i)|}{L * 9} \quad (1)$$

In Eq. 1, C is the degree of complementary hydropathy $H(i)$ and $H'(i)$ are the hydropathy indices of the

residues in the motif and target sequences respectively at position i , and L is the length of the motif. The degree of complementary hydropathy can range from 0 to 1. A predicted hit was considered good if the percent match was greater than 75% and the degree of complementary hydropathy was greater than 0.5.

To further predict the interactions between TREM2 and IL-34, we implemented protein-protein docking using HADDOCK [29] with TREM2 residues of R47, R62, L75, R76, and R77 that could cause at least a 2-fold decrease in K_D when mutated verse WT, as restraints. IL-34 domains that were predicted as potential binding sites for TREM2 from the hydropathy screening were set

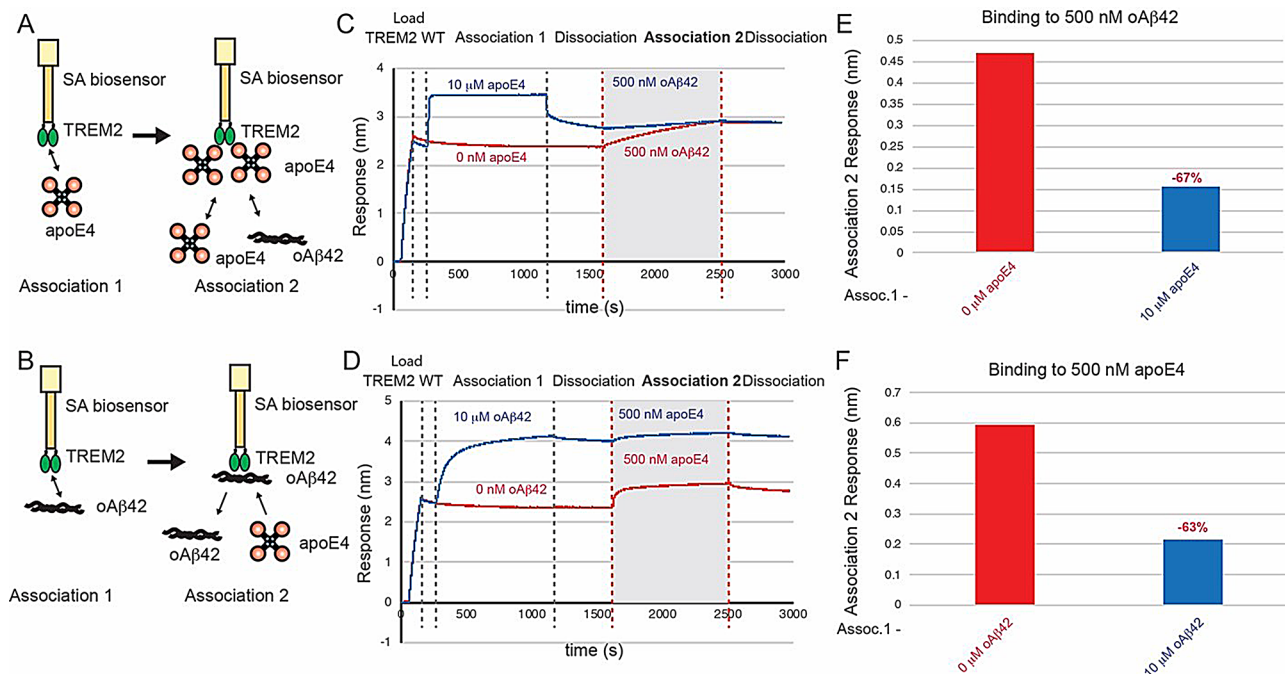


Fig. 3 ApoE4 and oAβ42 compete for binding to TREM2. **(A & B)** Schematic of competition binding BLI experiments. **(C & D)** BLI sensorgrams for **(C)** apoE4 competing oAβ42 binding to TREM2 and **(D)** oAβ42 competing apoE4 binding to TREM2. Red sensorgrams are TREM2 binding to **(C)** 500 nM oAβ42 or **(D)** 500 nM apoE4 alone while blue sensorgrams show competition experiments where **(C)** 10 μM apoE4 or **(D)** 10 μM oAβ42 are bound first. **(E & F)** BLI binding magnitudes for TREM2 binding to **(E)** 500 nM oAβ42 when pre-binding 10 μM apoE4 or **(F)** 500 nM apoE4 when pre-binding 10 μM oAβ42

as the preferred binding domains for TREM2 in protein-protein docking. Prior to docking, we energy minimized the IL-34 structure (PDBID: 4DKC [30]) in Amber18 and used a previously equilibrated TREM2 structure (PDBID: 5UD7 [22]). The hydrogen bond analysis and electrostatic surface potential analysis of the top predicted complex from HADDOCK was analyzed in PyMOL.

Results

Creation of a TREM2 variant protein library to comprehensively evaluate TREM2-ligand interactions

In order to comprehensively investigate the involvement of putative TREM2 binding surfaces in engaging various ligands, we designed a structure-guided library of TREM2 variants (Fig. 1). Due to the anionic or low pI nature of most TREM2 ligands, most variants were designed as mutations to aspartate (D) and most were point variants, with the exception of some double and triple mutants designed at each site (hydrophobic, basic, and site 2). In total, we have created 28 human TREM2 variants (Fig. 1). Human and mouse TREM2 Ig domains are 73% sequence identical and 87% similar. All the residues chosen for mutation are either identical or conserved in mouse, hence results using this library will be relevant to interpreting mouse model studies. All TREM2 variants were cloned into a vector that contained a specific biotinylation sequence at the C-terminus. Thus when immobilized on streptavidin-coated BLI

pins, these proteins are presented to ligands in the same orientation and oligomerization state as they are on the cell surface. All proteins were expressed in mammalian cells as we previously published [31], thus they contain similar post translational modifications (glycosylation and disulfide bonds) to the native proteins expressed by microglia. In order to characterize the oligomeric state of the expressed TREM2 ectodomains, we carried out size-exclusion chromatography coupled to multiangle light scattering (SEC-MALS). This analysis showed that sTREM2 WT is a monomer in solution (Supplemental Fig. 2). SEC analysis of TREM2 variants created for this study, such as sTREM2 L69D/L71D and sTREM2 W44D/L69D/L71D, demonstrated that they eluted at volumes similar to WT, indicated that the mutations introduced did not grossly impact folding or the monomeric state of the protein (Supplemental Fig. 3). This protein library represents a powerful tool for mapping TREM2 interactions with ligands. In this study, the purpose was to address which of the putative binding sites are involved in binding various TREM2 ligands, hence, not all variants were utilized to study each ligand.

Mutations to the TREM2 hydrophobic site can ablate binding to apoE4

In a previous study, we showed that apoE4 bound to TREM2 with the highest affinity compared to other apoE isoforms (TREM2-apoE4 K_D = 281 nM; TREM2-apoE3

$K_D = 440$ nM; TREM2-apoE2 $K_D = 590$ nM), thus apoE4 was used as the representative apoE isoform for binding studies. We also showed that AD risk variants in TREM2 (R47H, R62H, and T96K) did not grossly impact binding to apoE2, 3 or 4 [9]. Instead, we found that point mutations to the hydrophobic site, namely that mutants L69D and W70D, decreased binding affinity by nearly 200-fold (Fig. 2B; Table 1). In order to comprehensively extend these studies, we carried out further BLI experiments to complete characterizing the most common AD risk variants, and used TREM2 mutants at all three binding sites. Surprisingly, while the TREM2 AD variants R47H, R62H, and T96K had previously shown slight decreases in binding affinity for apoE4 (2–3 fold decrease in K_D , Table 1), we found that AD risk variant D87N showed a dramatic 11-fold increase in affinity for apoE4 ($K_D = 25$ nM; Fig. 2F; Table 1). This dramatic increase in affinity was also observed for the other apoE isoforms (TREM2 D87N - apoE2 $K_D = 52$ nM; TRME2 D87N - apoE3 $K_D = 79$ nM) (Supplemental Fig. 4). Next we evaluated the impact of double and triple mutations to the three putative binding surfaces on TREM2. Strikingly, we found that double (L69D/L71D) and triple (W44D/L69D/L71D) mutations at the hydrophobic site completely ablated binding to apoE4 (Fig. 2D, E; Table 1). TREM2 L69D/L71D also showed no binding to apoE2 or apoE3 (Supplemental Fig. 4). In stark contrast, double mutations to the basic site (R46A/R47A) and site 2 (R122D/K123D) did not did not largely impact binding to apoE4 (Fig. 2C & I, Table 1). Two point mutations in the basic site, R76D and R77D, did display 5-fold decreases in K_D for apoE4

(Fig. 2G, H, Table 1), suggesting that these residues might be partially involved in engaging apoE4. However, these residues are directly adjacent to the hydrophobic site, and might impact conformation of CDR2. In order to independently probe apoE4 engagement by TREM2, we also carried out binding assays by ELISA, which validated our results by BLI (Supplemental Fig. 5). In summary, our results suggest that apoE4 (as well as apoE2 and 3) primarily engages the hydrophobic site on TREM2.

ApoE and oA β 42 compete for binding to the TREM2

Since a previous study had suggested that apoE and oA β 42 might compete for binding to TREM2 [32], and our mapping studies indicated that apoE4 engages the hydrophobic site on TREM2, we conducted assays to examine if they compete for an overlapping binding site. In these competition binding assays, TREM2 was immobilized on the pin and then allowed to associate with 10 μ M of apoE4, then dipped into a well containing 500 nM oA β 42 (Fig. 3A). We found that apoE4 robustly inhibited the binding of oA β 42 to TREM2, reducing binding by 67%. (Fig. 3C, E). We then carried out the experiment in the opposite order, with TREM2 first binding to 10 μ M of oA β 42 (Fig. 3B). In this orientation, we found that oA β 42 also reduced binding by about 63% (Fig. 3D, F). We found that this result could be replicated across apoE2 and apoE3 isoforms as well (Supplemental Fig. 6). Since apoE and oA β 42 are also known to interact [33], we measured the affinity using BLI. We found oA β 42 bound to apoE proteins with slightly lower affinities than TREM2-apoE interactions (oA β 42 - apoE2 $K_D = 770$ nM; oA β 42 - apoE3 $K_D = 580$ nM; oA β 42 - apoE4 $K_D = 667$ nM) (Supplemental Fig. 7). Since these affinities are slightly lower than TREM2-apoE or TREM2-oA β 42 interactions, it is unlikely that apoE binding to oA β 42 causes dissociation from TREM2 or vice versa. Altogether, these results indicate that apoE4 and oA β 42 share an overlapping binding site on TREM2, suggesting that oA β 42 at least partially engages the hydrophobic site, and demonstrating that apoE4 and oA β 42 can both strongly compete for binding to TREM2.

Mutations to the TREM2 hydrophobic site severely inhibit binding to TDP-43

TDP-43 aggregate accumulations are found in most ALS patients, and are also found in individuals with FTD and AD. TREM2 was recently identified as a receptor for TDP-43 oligomers, with engagement triggering phagocytic clearance of TDP-43 oligomers by microglia [15]. In that report, direct interaction between TREM2 and soluble TDP-43 oligomers was demonstrated using SPR. In order to identify the binding site on TREM2 for oligomeric TDP-43, we prepared TDP-43 oligomers in a similar manner and used BLI to probe interactions with

Table 1 TREM2 variants binding to apoE4

TREM2 variant	K_D (nM)	Fold increase (\uparrow) or decrease (\downarrow) vs. WT
WT	281 \pm 43*	-
R47H	643 \pm 91*	\downarrow 2.29
R62H	561 \pm 117*	\downarrow 2.00
D87N	25 \pm 6	\uparrow 11.24
T96K	891 \pm 196*	\downarrow 3.17
M41D	1426 \pm 566*	\downarrow 5.07
W44D	2565 \pm 710*	\downarrow 9.12
L69D	55,060 \pm 20,390*	\downarrow 195.94
W70D	28,110 \pm 14,380*	\downarrow 100.04
F74D	9709 \pm 1163*	\downarrow 34.55
L69D/L71D	N.B.D.**	-
W44D/L69D/L71D	N.B.D.**	-
R76D	1529 \pm 693	\downarrow 5.44
R77D	1659 \pm 379	\downarrow 5.90
R46A/R47A	388 \pm 141	\downarrow 1.38
R122D/K123D	120 \pm 22	\uparrow 2.30

*Previously determined [9]

**N.B.D. = no binding detected

TREM2 variants across the three TREM2 binding sites. With TREM2 immobilized on the pin, we found that it bound TDP-43 robustly (Fig. 4A, B). Due to the oligomeric nature of TDP-43, binding curves were biphasic, so 1:1 kinetic fits were not appropriate; therefore, binding curves were only qualitatively evaluated. Mutations to the basic site (R47H, R62H, D87N) and site 2 resulted in binding magnitudes comparable to WT (Fig. 4G, H, I, K). A double mutant at the basic site (R46A/R47A) displayed slightly reduced binding (Fig. 4C, K). Similarly, double mutation R122D/K123D at site 2 resulted in slightly increased binding as compared to WT (Fig. 4J, K). In stark contrast, single (W70D), double (L69D/L71D), and triple mutations (W44D/L69D/L71D) to the hydrophobic site completely ablated binding to TDP-43 (Fig. 4D, E, F, K). Altogether, these results suggest that TDP-43

oligomers engage TREM2 at the hydrophobic site near residue 70.

Mutations to the TREM2 basic site inhibit binding to C1q, while hydrophobic site mutations partially impair binding C1q is known to form a complex with TREM2 which consequently inhibits formation of the classical complement cascade [20]. We found that TREM2 binds to C1q with moderately high affinity, $K_D = 650$ nM (Fig. 5A, B; Table 2). This is two orders of magnitude weaker than the K_D of 7.35 nM recently reported from ELISA experiments [20]. We first probed mutations to the hydrophobic site, and found that most mutations slightly impaired binding, including M41D, L69D, W70D, L71D, and L89D (Fig. 5C–F, I; Table 2). A triple mutation at the hydrophobic site, W44D/L69D/L71D, appeared to partially impair binding

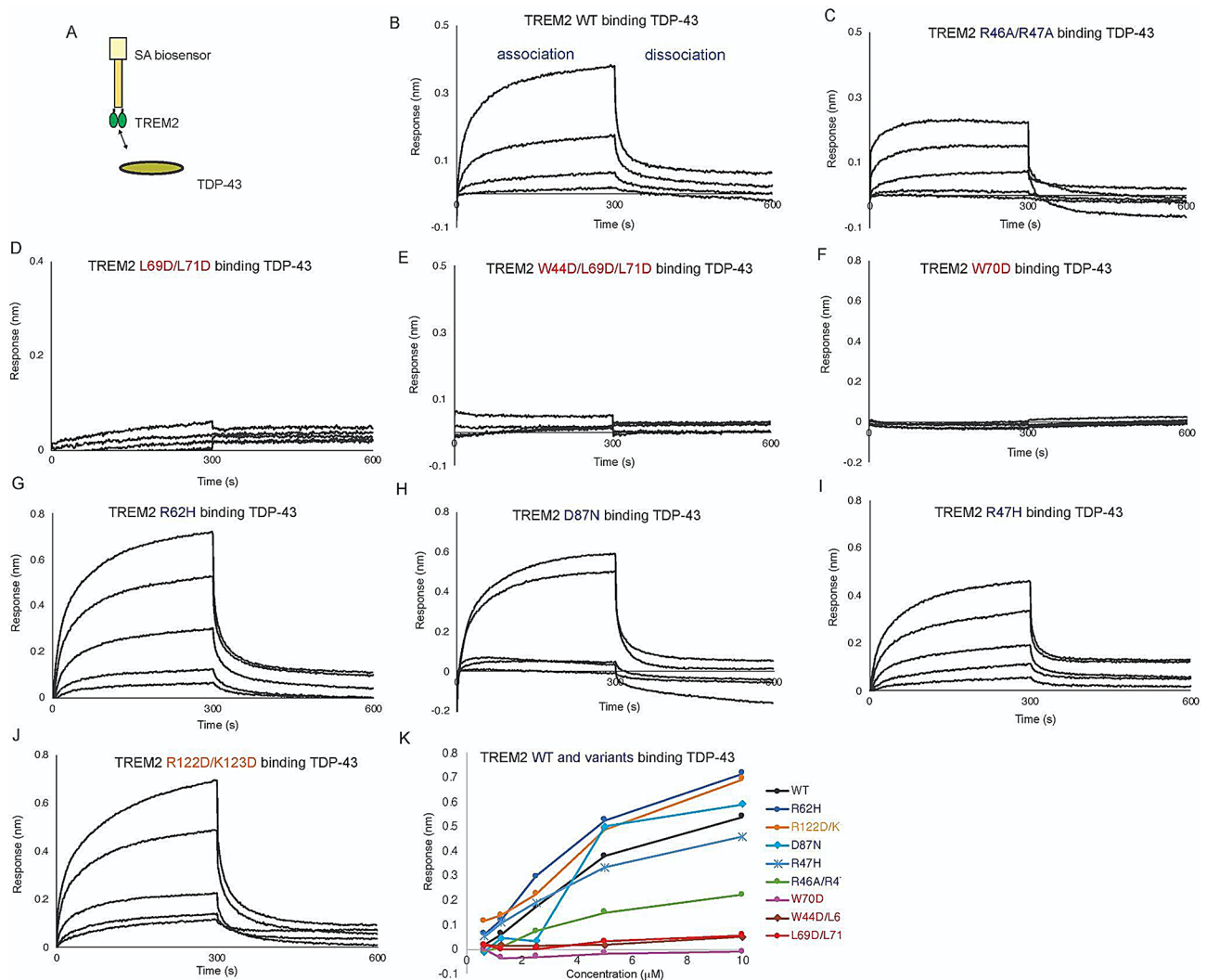


Fig. 4 Mutations to TREM2 hydrophobic site ablate binding to TDP-43. Immobilized TREM2 WT and variants were probed for binding to TDP-43 (0.625–10 μ M). (A) Scheme of experiment. (B–F) BLI response for TREM2 (B) WT, (C) R46A/R47A, (D) L69D/L71D, (E) W44D/L69D/L71D, (F) W70D, (G) R62H, (H) D87N, (I) R47H, (J) R122D/K123D binding to TDP-43 (0.625–10 μ M). Double-reference subtracted data (black) is shown. (K) Summary of BLI steady-state binding response versus concentration for TDP-43 binding to TREM2 variants

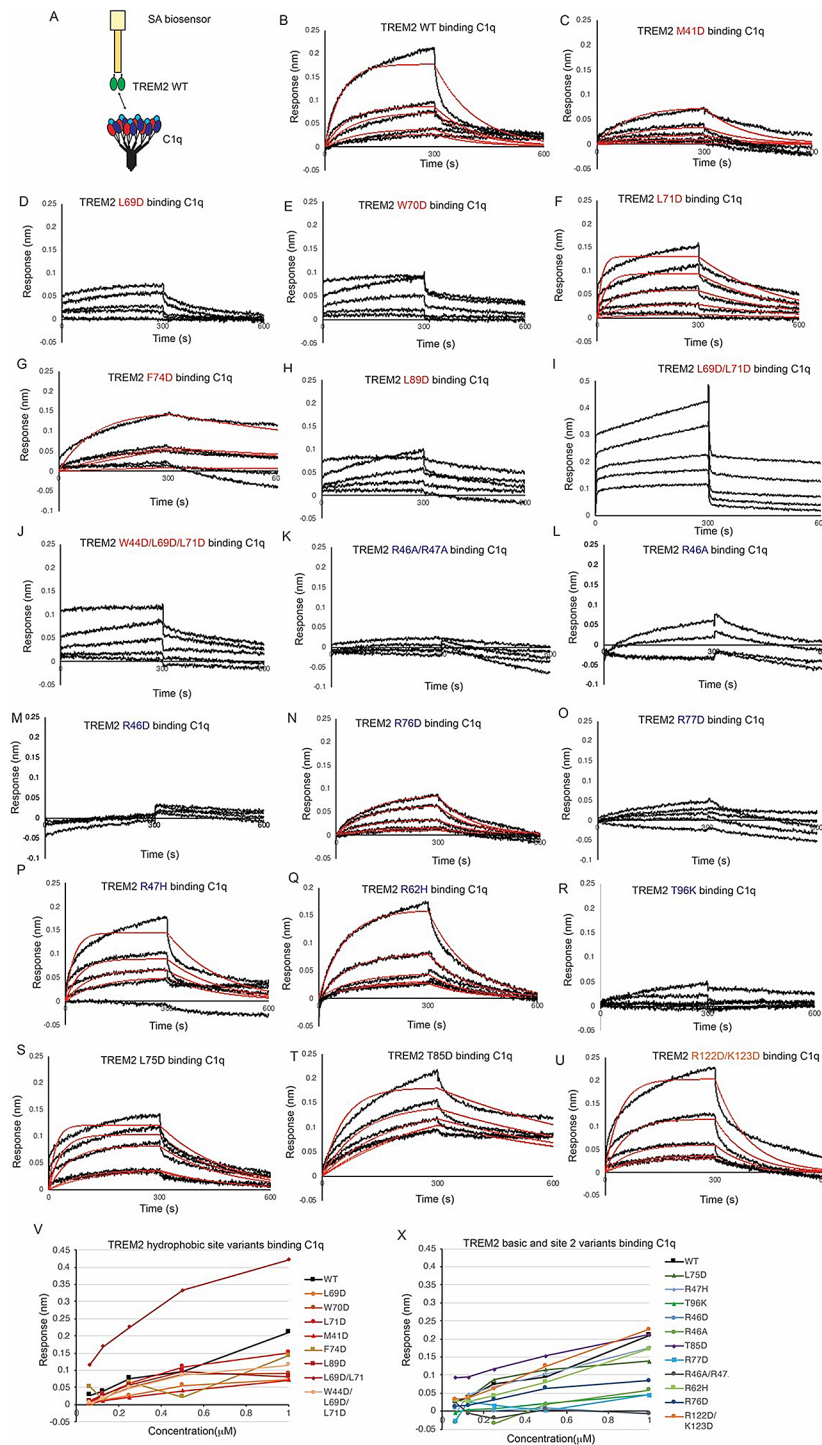


Fig. 5 C1q binding to TREM2 is mainly disrupted by TREM2 basic site variants. Immobilized TREM2 was probed for binding to C1q (62.5–1000 nM). **(A)** Scheme of experiment. **(B–N)** BLI sensorgrams for C1q binding to TREM2 **(B)** WT, **(C)** M41D, **(D)** L69D, **(E)** W70D, **(F)** L71D, **(G)** F74D, **(H)** L89D, **(I)** L69D/L71D, **(J)** W44D/L69D/L71D, **(K)** R46A/R47A, **(L)** R46A, **(M)** R46D, **(N)** R76D, **(O)** R77D, **(P)** R47H, **(Q)** R62H, **(R)** T96K, **(S)** L75D, **(T)** T85D, **(U)** R122D/K123D. Black = BLI sensorgrams; red = 1:1 kinetic fits. Results shown in Table 2. **(V–X)** Summary of BLI steady-state binding response versus concentration for C1q binding to TREM2 **(V)** hydrophobic site variants and **(X)** basic site variants

Table 2 TREM2 variants binding to C1q

TREM2 variant	K_D (μ M)
WT	0.65 \pm 0.03
M41D	2.54 \pm 0.52
L69D	Decreased binding
W70D	Decreased binding
L71D	0.058 \pm 0.002
F74D	0.11 \pm 0.01
L89D	Decreased binding
L69D/L71D	Binding (not fit)
W44D/L69D/L71D	Binding (not fit)
R46A/R47A	No Binding
R46A	No Binding
R46D	No Binding
R47H	0.18 \pm 0.01
R62H	1.66 \pm 0.06
R76D	13.8 \pm 4.86
R77D	No Binding
T96K	No binding
L75D	0.11 \pm 0.01
T85D	0.11 \pm 0.01
R122D/K123D	0.82 \pm 0.04

(Fig. 5J). Interestingly, the F74D and L69D/L71D variants appeared to show increased affinity for C1q (Fig. 5G, I; Table 2). In contrast, some mutations to the basic site dramatically impair binding, including R46A/R47A, R46A, R46D, R76D, and R77D (Fig. 5K-O; Table 2). Most notably, TREM2 R46A, R46D, and R46A/R47A show nearly complete ablated binding to C1q, suggesting a central importance for R46 in mediating this interaction. Mutations adjacent to the basic site, L75D and T85D, or mutations to site 2 (R122D/K123D) did not impair binding (Fig. 5S-U; Table 2). Notably, the AD risk variants R47H and R62H did not alter binding to C1q (Fig. 5P, Q; Table 2). In contrast, the TREM2 AD risk variant T96K showed no binding to C1q (Fig. 5R; Table 2). Altogether, our data indicate that TREM2 utilizes a surface on the basic site involving R46 and R77 to engage C1q, with extended contacts in the hydrophobic site.

Competition binding experiments with C1q, oA β 42, and apoE4 support an extended binding site of C1q

Since our BLI data indicated that C1q binds to an extended surface on TREM2, including residues in both the basic and hydrophobic sites, we hypothesized that AD ligands apoE4 and oA β 42 might compete with C1q for binding. We conducted BLI competition experiments to examine the relationship between binding of C1q, apoE4, and oA β 42. First, we investigated the ability of apoE4 and C1q to compete with each other for binding to TREM2 (Fig. 6A-F). We found that when apoE4 was first bound to TREM2, there was no binding signal for 1000 nM C1q (Fig. 6C, E), indicating that apoE4 could

block C1q binding to TREM2. Conversely, when TREM2 was first exposed to 1000 nM C1q, binding to apoE4 was nearly unaffected as compared to no C1q (3% decrease) (Fig. 6D, F), indicating that C1q is not able to block apoE4 binding to TREM2. These results suggest that apoE4 may share an overlapping binding site with C1q, although C1q is not able to compete off apoE4. We observed similar results in competition binding experiments using apoE2 (Supplemental Fig. 8). We next investigated the ability of oA β 42 and C1q to compete with each other for binding to TREM2 (Fig. 6G-L). We observed that when TREM2 was first exposed to 500 nM oA β 42, there was a 66.7% reduction in binding of C1q to TREM2 (Fig. 6I, K). Correspondingly, when TREM2 was first exposed to 1000 nM C1q, minimal inhibition (22%) of 500 nM oA β 42 binding to TREM2 was observed (Fig. 6J, L). Taken together, our results support the observation that C1q at least partially engages the hydrophobic site on TREM2, since both apoE4 and oA β 42 can block C1q from engaging it. They also show that both apoE4 and oA β 42 can out compete C1q for binding to TREM2, likely due to the lower affinity of the C1q-TREM2 interaction (K_D = 650 nM) as compared to apoE4 (K_D = 280 nM) [9] and oA β 42 (K_D = 42 nM) (Supplemental Fig. 9).

Mutations to the TREM2 basic site around R76 severely inhibit binding to IL-34

IL-34 was recently identified as a signaling ligand for TREM2 [18]. In order to map the binding surface for IL-34 on TREM2, we carried out BLI binding studies with our TREM2 variant library. With TREM2 WT immobilized on the BLI pin, we found that IL-34 bound with high affinity (K_D = 16.5 nM) (Fig. 7A, B; Table 3). In contrast to the other ligands studied here, IL-34 bound to some TREM2 AD risk variants (R47H, R62H) with slightly lower affinity, showing around a 4-fold decrease in K_D (Fig. 7C, I Table 3). The AD risk variants D87N and T96K did not largely impact IL-34 binding (Fig. 7D, E; Table 3). We further probed the basic site and found that the R77D variant showed a nearly 7-fold decrease in affinity (K_D = 114 nM, Fig. 7K; Table 3) while the R76D mutant displayed no binding to IL-34 at the concentration range probed (Fig. 7J; Table 3). We further probed this region and introduced mutations at residues adjacent to R76. These variants (L75D, W78D, T85D) did not impact binding to IL-34 (Fig. 7L-N; Table 3). Another mutation to the basic site, R46D, also did not impact binding to IL-34 (Fig. 7F; Table 3). We then probed mutations at the hydrophobic site and site 2. The site 2 variant (R122E) did not impact binding (Fig. 7O), nor did the site 2 double mutant R122D/K123D (Fig. 7P). Most notably, the double and triple hydrophobic site variants L69D/L71D (Fig. 7H) and W44D/L69D/L71D (Fig. 7G) did not affect binding to IL-34. Additionally, these results further

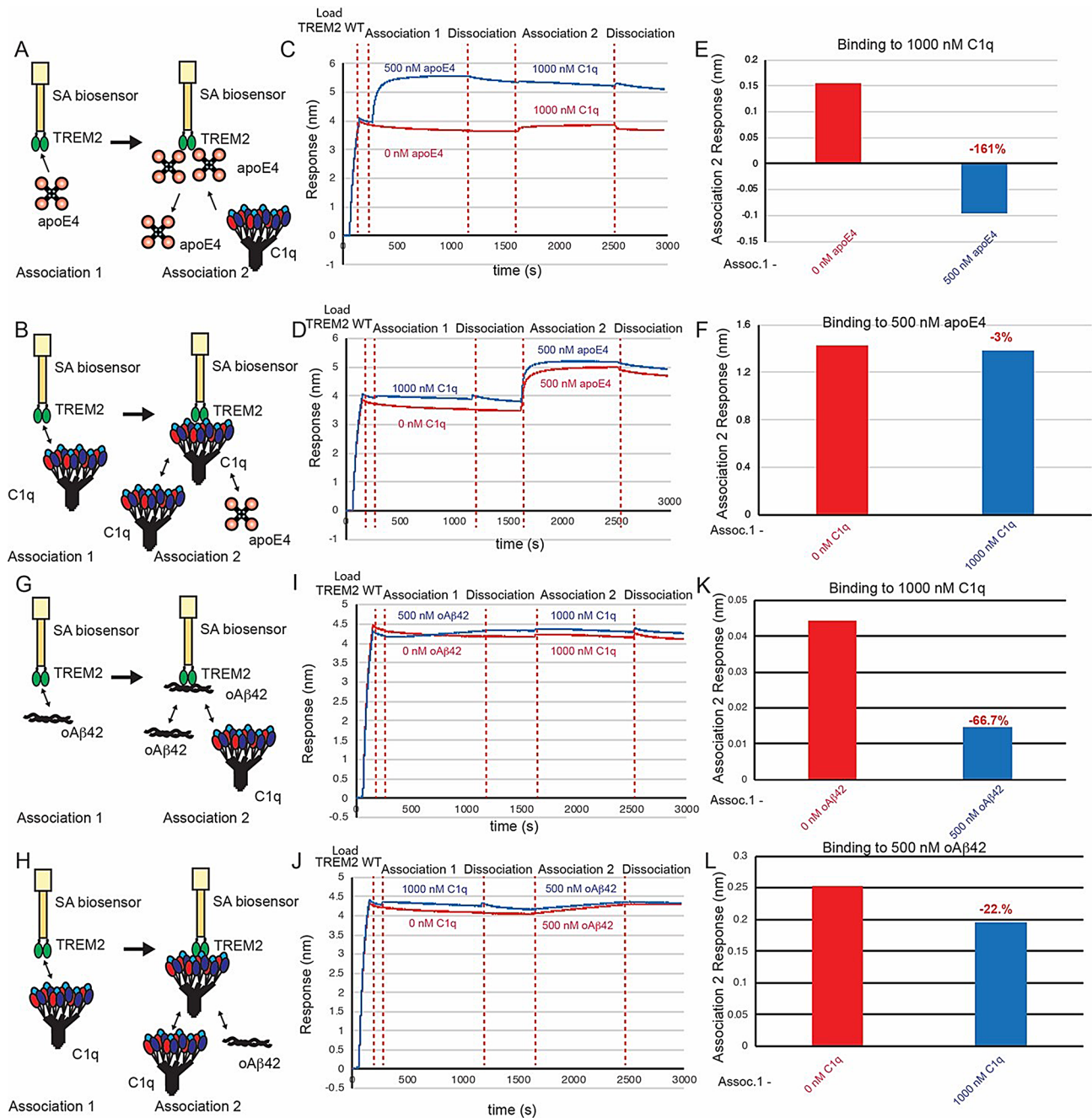


Fig. 6 C1q minimally competes with apoE4 and oAβ42 for binding to TREM2. **(A&B)** Schematic of competition binding BLI experiments. **(C&D)** BLI sensorgrams for **(C)** apoE4 competing C1q binding to TREM2 and **(D)** C1q competing apoE4 binding to TREM2. Red sensorgrams are TREM2 binding to **(C)** 1000 nM C1q or **(D)** 500 nM apoE4 alone while blue sensorgrams show competition experiments where **(C)** 500 nM apoE4 or **(D)** 1000 nM C1q are bound first. **(E&F)** BLI binding magnitudes for TREM2 binding to **(E)** 1000 nM C1q alone or when pre-binding 500 nM apoE4 or **(F)** 500 nM apoE4 alone or when pre-binding 1000 nM C1q. Percent decrease in Association 2 binding signal in the presence of the competitor is shown above the bars. **(G & H)** Schematic of competition binding BLI experiments. **(I&J)** BLI sensorgrams for **(I)** oAβ42 competing C1q binding to TREM2 and **(J)** C1q competing oAβ42 binding to TREM2. Red sensorgrams are TREM2 binding to **(I)** 1000 nM C1q or **(J)** 500 nM oAβ42 alone while blue sensorgrams show competition experiments where **(I)** 500 nM oAβ42 or **(J)** 1000 nM C1q are bound first. **(K&L)** BLI binding magnitudes for TREM2 binding to **(K)** 1000 nM C1q alone or when pre-binding 500 nM oAβ42 or **(L)** 500 nM oAβ42 alone or when pre-binding 1000 nM C1q. Percent decrease in Association 2 binding signal in the presence of the competitor is shown above the bars

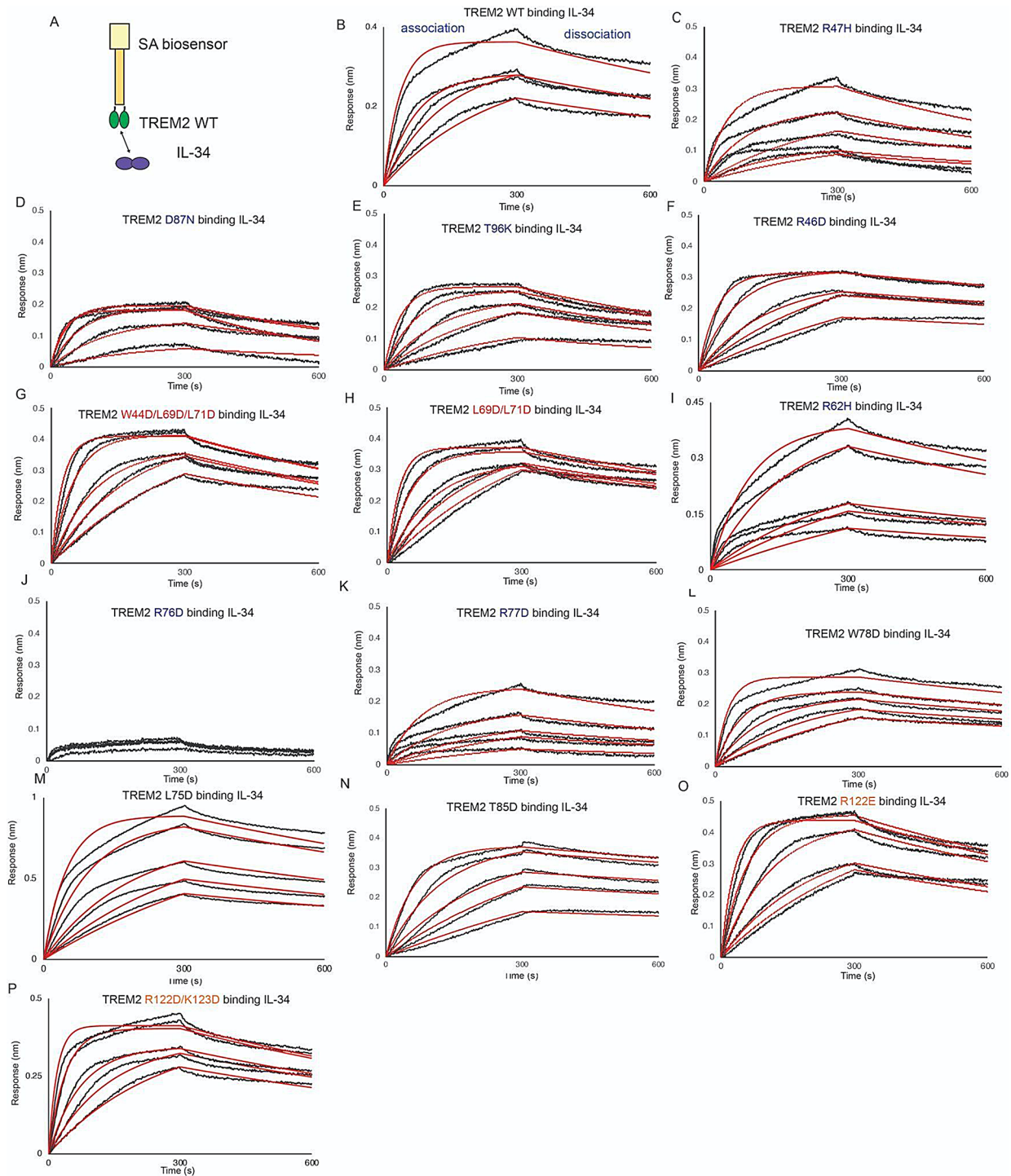


Fig. 7 TREM2 basic site variants centered around R76 inhibit binding to IL-34. Immobilized TREM2 was probed for binding to IL-34 (62.5–1000 nM). **(A)** Scheme of experiment. **(B–N)** BLI sensorgrams for IL-34 binding to TREM2 **(B)** WT, **(C)** R47H, **(D)** D87N, **(E)** T96K, **(F)** R46D, **(G)** W44D/L69D/L71D, **(H)** L69D/L71D, **(I)** R62H, **(J)** R76D, **(K)** R77D, **(L)** W78D, **(M)** L75D, **(N)** T85D, **(O)** R122E, **(P)** R122D/K123D. Black = BLI sensorgrams; red = 1:1 kinetic fits. Results shown in Table 3

Table 3 TREM2 variants binding to IL-34

TREM2 variant	K _D (nM)	Fold decrease vs. WT
WT	16.5±0.2	-
R47H	79.8±2.4	↓4.8
R62H	75	↓4.5
D87N	28.4±0.5	↓1.7
T96K	23.7±0.4	↓1.4
R46D	18.0±0.3	↓1.1
R76D	N.B.D	-
R77D	114±4	↓6.9
L75D	36.6±0.9	↓2.2
W78D	17.2±0.4	↓1.04
T85D	21.5±0.6	↓1.3
R122E	29.4±0.4	↓1.8
R122D/K123D	18.5±0.3	↓1.1
L69D/L71D	20.2±0.3	↓1.2
W44D/L69D/L71D	25.8±0.3	↓1.6

validate that L69D/L71D double and W44D/L69D/L71D triple mutants are not grossly misfolded, as indicated by SEC analysis (Supplemental Fig. S3). These results suggest that IL-34 binds to the TREM2 basic site in a region centered on R76.

A predicted structure for the TREM2/IL-34 complex

A recent manuscript presented a computational prediction for the TREM2/IL-34 complex [18]. In this report, IL-34 was predicted to bind TREM2 at the hydrophobic site, with contact residues including W44, W70, and L71. However, our experimental results show that mutations to the hydrophobic site do not impact binding to TREM2, and instead show that the IL-34 binding site is on the basic site, centered on R76. Therefore, we further undertook computational prediction of the binding sites between TREM2 and IL-34 to support our experimental data.

We first identified key residues of TREM2 and IL-34 that were most likely involved in protein-protein interactions using a machine learning and homology-based inference approach [25]. In TREM2, 14 residues were identified as likely involved in binding. These include residues in CDR1 (residues 40–42) and CDR2 (residues 69–72) as well as basic site residues (residues 66–68 and 112–114) (Fig. 8A). The residues predicted around CDR2 are directly surrounded by residues that can strongly inhibit IL-34 binding when mutated (Table 3) including R62, R76, and R77. Both residues 112–114 and residues 66–68 are spatially adjacent to another residue, R47, that can strongly inhibit IL-34 binding when mutated. In IL-34 there were 34 residues identified as likely involved in protein-protein binding. These residues existed primarily at the end of Helix 1, the beginning of Helix 4, and throughout Helix 6, suggesting the binding likely occurs in the helix bundle (Fig. 8B).

To further identify regions of TREM2 and IL-34 that could be responsible for binding, we used a sequence-based hydrophathy mapping approach. The structure of IL-34 can be broken into six helices. Each helix sequence was screened against the sequence of TREM2 immunoglobulin (Ig) domain to identify potential regions of binding. Scanning both the forward and reverse residue sequences of the six helices, hits with more than 75% percent match and greater than 0.5 degree of complementary hydrophathy were considered successful. Based on our criteria, helices 2, 5, and 6 all had good hits targeting a combination of TREM2 basic site and TREM2 CDR2 (Table S1). When the successful hits were clustered on the TREM2 sequence, we found two regions for predicted binding, residues 49–82 and residues 112–127 (Fig. 8A). These two strands contain most of the residues in the basic site, as well as the entirety of CDR2, consistent with the BLI results (Table 3). Similarly, we screened the three TREM2 CDR loops (hydrophobic regions – CDR1: 39–46, CDR2: 69–75, CDR3: 88–91) as well as the four TREM2 strands that make up the basic site (residues 47–50, 62–68, 76–78, and 112–114) separately across the sequence of IL-34 to identify potential binding regions between TREM2 and IL-34. We scanned both the forward and reverse residue sequences of the three CDR loops and four basic site strands in TREM2 against the sequence of IL-34, where hits with more than 75% percent match and greater than 0.5 degree of complementary hydrophathy were considered successful. From these results, we noted the largest amount of good hits came from the basic site residues, as well as CDR2 in TREM2 (Table 2). This again matches well with our predicted binding regions on TREM2, as well as the BLI results, which showed mutations of the residues from TREM2 basic site were able to strongly disrupt TREM2/IL-34 binding (Table 3). We clustered the good hits on the sequence of IL-34 and noted five regions of potential interest were identified: Helix 2 (residues 71–85), Helix 3 (residues 90–100), Helix 4 (residues 119–129), Helix 5 (residues 142–151), and Helix 6 (residues 156–179) (Fig. 8B). Of these five regions, the residues in helices 3, 4, and 5 primarily make up the negatively charged surface of IL-34 while residues in helices 2 and 6 make up IL-34 positively charged surface (Fig. 8C).

To further narrow down the IL-34 binding site for TREM2, we predicted TREM2/IL-34 complex structure using HADDOCK [29] with BLI results of TREM2 binding site for IL-34 as restraint. Our protein-protein docking results show the negatively charged surface of IL-34 (Helices 3, 4, and 5) interacted with the positively charged basic site of TREM2 (Fig. 8C-D). The TREM2 binding site for IL-34 included the four key TREM2 residues of R47, R62, R76, and R77 whose mutation could greatly inhibit TREM2/IL-34 interactions when mutated

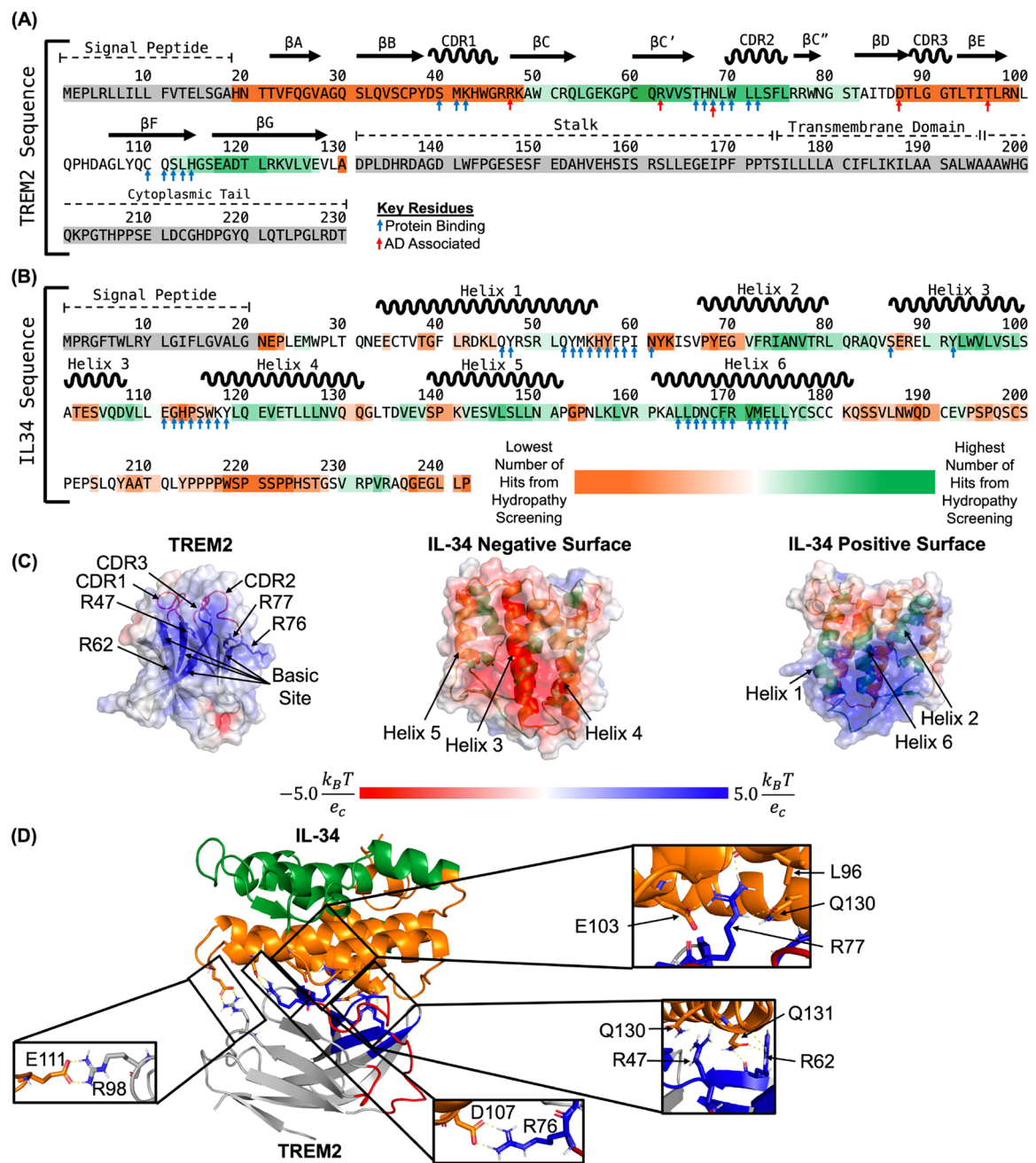


Fig. 8 (See legend on next page.)

(See figure on previous page.)

Fig. 8 Computational prediction of the interactions between TREM2 basic site and IL-34 negatively charged surface. **(A)** The complete sequence of human TREM2 showing predicted potential key residues and binding regions between residues 49–82 and 112–127 (Basic site and CDR2) for IL-34. Blue arrows denote residues predicted to be important for protein binding via PredictProtein and red arrows denote residues that increase Alzheimer's disease risk. Residues in TREM2 immunoglobulin domain are highlighted ranging from orange to green. Residues highlighted in the darkest green had the highest number of hits and residues highlighted in the darkest orange had the lowest number of hits. Residues highlighted in grey were not screened. **(B)** The complete sequence of IL-34 showing predicted potential key residues and binding regions between residues 71–85, 90–100, 119–129, 142–151, and 156–179 for TREM2. Blue arrows denote residues predicted to be important for protein binding via PredictProtein. Residues highlighted in the darkest green had the highest number of hits and residues highlighted in the darkest orange had the lowest number of hits. Residues highlighted in grey were not screened. **(C)** Electrostatic surface potential maps showing positively charged TREM2 basic site, negatively charged IL34 surface (made up of helices 3, 4, and 5), and positively charged IL34 surface (made up of helices 1, 2, and 6). Regions with positive electrostatic surface potential are shown as blue, regions with negative electrostatic surface potential are shown as red, and neutral regions are shown as white. TREM2 is shown as grey with the basic site shown as blue cartoon and the hydrophobic site shown as red cartoon. Key regions and residues for binding are labeled. IL-34 is shown as cartoon with residues making up the negatively charged surface colored in orange and residues making up the positively charged surface colored in green. The six helices are labeled. **(D)** Predicted complex structure of TREM2 with IL-34 shows the negatively charged surface of IL-34 (helices 3, 4, and 5) interaction with the positively charged basic site of TREM2, and key TREM2 residues identified through BLI forming hydrogen bonds and salt bridges with IL-34 residues. TREM2 is shown in gray, TREM2 basic site is shown as blue, and TREM2 hydrophobic site is shown as red. Residues making up IL-34 negatively charged surface are shown as orange and residues making up IL-34 positively charged surface are shown as green. Hydrogen bonds and salt bridges between key identified TREM2 residues from BLI and residues from IL-34 are shown as sticks and the interactions are shown as dashed yellow lines

as observed in BLI results. In the predicted TREM2/IL-34 complex structure (Fig. 8D), TREM2 residues R47, R62, and R77 all formed hydrogen bonds with residues in IL-34 (Fig. 8D). Additionally, TREM2 residue R76 formed a salt bridge with IL-34 residue D107 (Fig. 8D). This interaction is particularly interesting as the loss of the salt bridge when R76 is mutated to aspartic acid could be a driving factor for complete loss of binding in this mutation. Further, the mutations to R47, R62, and R77 could all reduce or inhibit the formation of key hydrogen bonds that could result in reduced interactions. In our model we also noted TREM2 residue R98 formed a salt bridge with IL-34 residue E111 (Fig. 8D). The mutation R98W has previously been identified in AD patients and the R98W TREM2 variant may be associated with AD [2]. The mutation of arginine to tryptophan would break the salt bridge with IL-34 and could potentially reduce TREM2/IL-34 interactions. Our computational results strongly suggest that the negatively charged surface of IL-34 (helices 3, 4, and 5) directly binds to and interacts with the TREM2 positively charged basic site.

Competition experiments support that IL-34 binds to a site adjacent to those occupied by apoE4 or $\alpha\beta 42$

Since our binding studies indicated that IL-34 did not bind to the hydrophobic site and instead engaged a surface on the basic site centered on R76, we hypothesized that TREM2 might be able to bind to both IL-34 and either apoE4 or $\alpha\beta 42$ simultaneously. To determine the relationship between binding sites for IL-34, apoE4, and $\alpha\beta$, we employed competition binding experiments by BLI similar to those we had done for apoE4 and $\alpha\beta 42$ (Fig. 9). First, we investigated competition between IL-34 and apoE4. We found that when TREM2 was first exposed to 500 nM apoE4 and then dipped in 500 nM IL-34, binding to IL-34 was reduced by 61% (Fig. 9A, C,E). When TREM2 was first exposed to 500 nM IL-34

and dipped into 500 nM apoE4, binding to apoE4 was reduced by 15% (Fig. 9B, D,F). These results suggest that apoE4 and IL-34 exhibit some degree of steric hindrance upon binding to TREM2, which likely occurs due to the proximity of R76 to the hydrophobic site. We next investigated competition between IL-34 and $\alpha\beta 42$. When TREM2 was first exposed to 500 nM $\alpha\beta 42$, binding to 500 nM IL-34 was only reduced by 19% (Fig. 9G, I,K). When TREM2 was first exposed to 500 nM IL-34, binding to $\alpha\beta 42$ was marginally reduced by 5% (Fig. 9H, J,L). These results suggest that IL34 and $\alpha\beta 42$ only slightly compete for binding to TREM2, suggesting little, if any, overlap of binding sites. Altogether, the results support that IL-34 binds a site adjacent to the hydrophobic sites engaged by apoE4 and $\alpha\beta 42$.

Competition experiments support that IL-34 and C1q compete for adjacent binding surfaces in the basic site

Since our binding studies indicated that both IL-34 and C1q primarily engaged the basic site, we hypothesized that their binding sites might overlap. To examine the relationship between binding sites for IL-34 and C1q, we employed competition binding experiments (Fig. 9M-R). We found that when TREM2 was first exposed to 500 nM IL-34 and then dipped in 1000 nM C1q, binding to C1q was completely blocked (Fig. 9M, O,Q). When TREM2 was first exposed to 1000 nM C1q and then dipped into 500 nM IL-34, binding to IL-34 was reduced by over half (54%) (Fig. 9N, P,R). These results suggest that the binding surfaces for IL-34 and C1q on the basic site of TREM2 exhibit some overlap-which may be limited due to the extensive interface engaged by C1q.

Discussion

TREM2 was first linked to AD by GWAS studies that identified rare point mutations in TREM2 as significant risk factors for developing AD [2, 4]. At that time, there

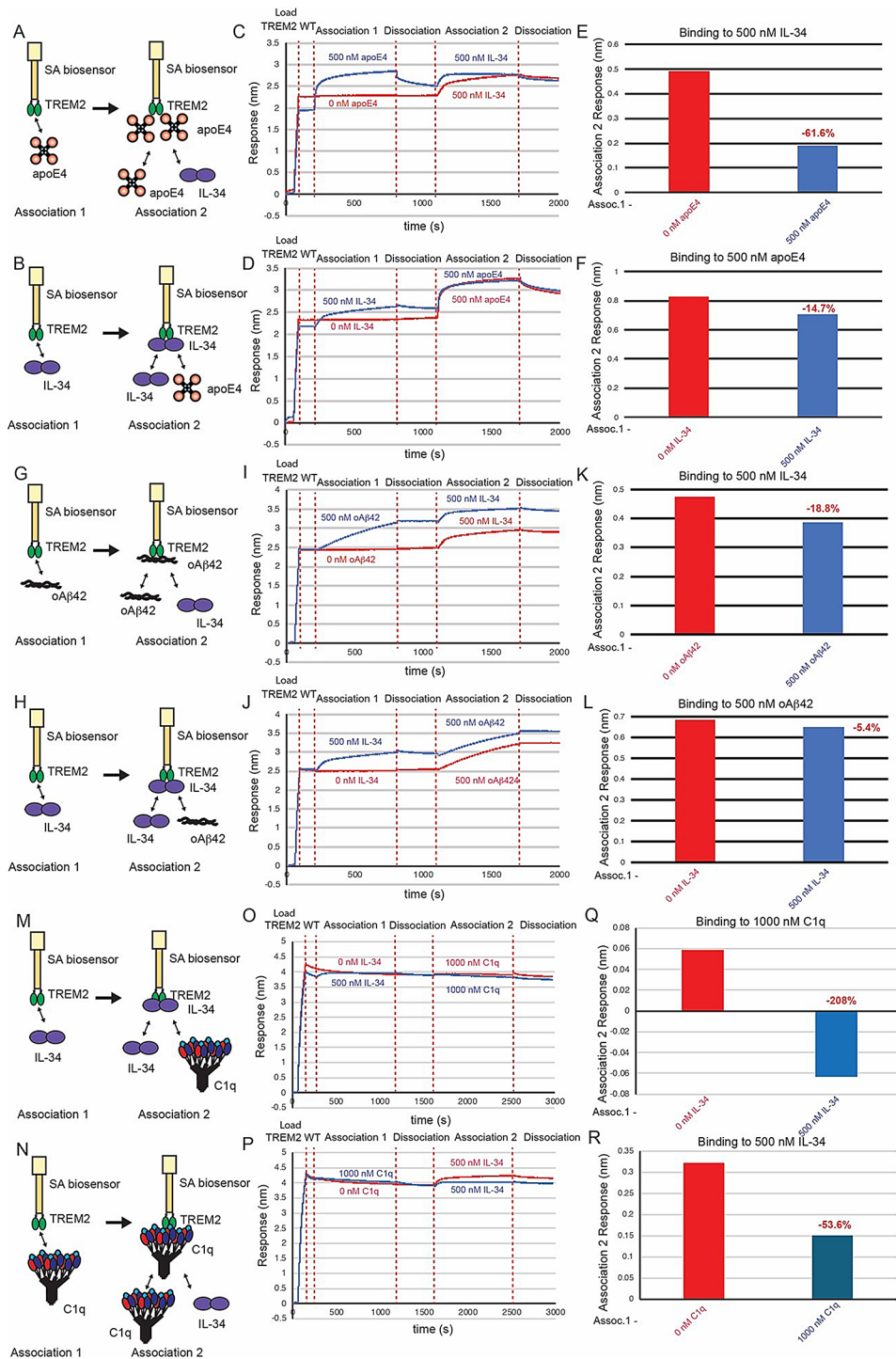


Fig. 9 (See legend on next page.)

(See figure on previous page.)

Fig. 9 C1q and apoE4 compete IL-34 for binding to TREM2, but $\alpha\beta 42$ does not compete IL-34 for binding to TREM2. **(A&B)** Schematic of competition binding BLI experiments. **(C&D)** BLI sensorgrams for **(C)** apoE4 competing IL-34 binding to TREM2 and **(D)** IL-34 competing apoE4 binding to TREM2. Red sensorgrams are TREM2 binding to **(C)** 500 nM IL-34 or **(D)** 500 nM apoE4 alone while blue sensorgrams show competition experiments where **(C)** 500 nM apoE4 or **(D)** 500 nM IL-34 are bound first. **(E&F)** BLI binding magnitudes for TREM2 binding to **(E)** 500 nM IL-34 alone or when pre-binding 500 nM apoE4 or **(F)** 500 nM apoE4 alone or when pre-binding 500 nM IL-34. Percent decrease in Association 2 binding signal in the presence of the competitor is shown above the bars. **(G & H)** Schematic of competition binding BLI experiments. **(I&J)** BLI sensorgrams for **(I)** IL-34 competing $\alpha\beta 42$ binding to TREM2 and **(J)** $\alpha\beta 42$ competing IL-34 binding to TREM2. Red sensorgrams are TREM2 binding to **(I)** 500 nM IL-34 or **(J)** 500 nM $\alpha\beta 42$ alone while blue sensorgrams show competition experiments where **(I)** 500 nM $\alpha\beta 42$ or **(J)** 500 nM IL-34 are bound first. **(K&L)** BLI binding magnitudes for TREM2 binding to **(K)** 500 nM IL-34 alone or when pre-binding 500 nM $\alpha\beta 42$ or **(L)** 500 nM $\alpha\beta 42$ alone or when pre-binding 500 nM IL-34. Percent decrease in Association 2 binding signal in the presence of the competitor is shown above the bars. **(M&N)** Schematic of competition binding BLI experiments. **(O&P)** BLI sensorgrams for **(O)** IL-34 competing C1q binding to TREM2 and **(P)** C1q competing IL-34 binding to TREM2. Red sensorgrams are TREM2 binding to **(O)** 1000 nM C1q or **(P)** 500 nM IL-34 alone while blue sensorgrams show competition experiments where **(O)** 500 nM IL-34 or **(P)** 1000 nM C1q are bound first. **(Q&R)** BLI binding magnitudes for TREM2 binding to **(Q)** 1000 nM C1q alone or when pre-binding 500 nM IL-34 or **(R)** 500 nM IL-34 alone or when pre-binding 1000 nM C1q. Percent decrease in Association 2 binding signal in the presence of the competitor is shown above the bars

were few known ligands for TREM2, outside of DNA and bacterial cell membrane debris [34]. Since then, a number of TREM2 ligands with relevance to AD have been identified. These ligands can all be classified as associated with tissue damage, and TREM2 could be classified as a scavenger receptor [35]. In this study, we begin to unravel the binding surfaces utilized by this promiscuous receptor.

The hydrophobic site on TREM2 appears to be a major binding site for most ligands. Here, we found that double and triple mutations to the hydrophobic site could ablate binding to apoE4 and TDP-43, whereas double mutations to the basic site only mildly impaired binding to these ligands. Competition experiments between apoE4 and $\alpha\beta 42$ indicate that they share overlapping binding sites, suggesting that $\alpha\beta 42$ at least partially engages the hydrophobic site. This is in agreement with previous competitive binding experiments by BLI which also demonstrated this [32]. In that study, $\alpha\beta 42$ was shown to completely block apoE4 from binding to TREM2, however concentrations were not reported. In our study we found that apoE4 and $\alpha\beta 42$ could both compete for binding at the hydrophobic site (Fig. 3). C1q also appears to partially utilize the hydrophobic site since some mutations strongly decrease binding. The hydrophobic site is composed mostly of residues from the CDR1, CDR2, and CDR3 loops. Our molecular dynamics simulations indicate that these loops represent the most conformationally dynamic region of TREM2 [36], further suggesting this region could structurally adjust to engage diverse ligands.

The TREM2 basic site appears to be the major surface engaged by C1q and IL-34. In the case of C1q, we found that variants with mutations at R46 displayed little or no binding to TREM2, and also found that mutations to R76 and R77 greatly impacted binding. These findings are in agreement with previous studies showing that a TREM2 31–71 peptide could bind C1q and inhibit the classic complement cascade [20]. Mutations to the hydrophobic site also impact binding to C1q but to a lesser degree, suggesting that C1q may engage in extended contacts with TREM2. C1q is a hexamer of trimers, composed of

18 total polypeptide chains. Due to the relatively large size of C1q, it is plausible for it to bind to an extended surface on TREM2. For IL-34, we found that mutations at R76 completely ablated binding, and mutations to R77 also impacted binding. This observation is consistent with previous structural studies of IL-34 in complex with its receptors. In these studies, electrostatic contacts between IL-34 and its receptors appear to drive complex formation. For example, the IL-34 dimer contains two pronounced electronegative surfaces that pair with large electropositive surfaces on the receptor, such as CSF1R [30]. Our experiments suggest that is also the case with TREM2 binding of IL-34, and are consistent with previous demonstrations that TREM2 and CSF1R can compete for binding to IL-34 [18].

In this study, we developed an extensive protein array of TREM2 variants that could be used to map binding to ligands. This array represents a powerful tool that can be used to map binding of TREM2 to newly discovered endogenous ligands and candidate small molecule therapeutics. In addition to utilizing structurally designed TREM2 variants to map binding to ligands, we also investigated the major TREM2 AD risk variants R47H, R62H, D87N, and T96K. In general, we have observed that the disease variants only mildly impact binding to ligands, and are generally not loss-of-function mutations [9, 21]. There are some exceptions to this, however. For example, in this study we found that the TREM2 D87N interaction with apoE4 displayed a greater than 10 fold increase in K_D compared to WT, representing a gain-of-function. This is consistent with the observation that TREM2 D87N shows a dramatic increase in signaling in response to apolipoprotein ligands [37]. Another exception is TREM2 T96K, which displays no binding to C1q. In general, our observations indicate that TREM2 AD variants only subtly impact interactions with these identified ligands, and their functional ramifications are likely nuanced or related to other as-yet undiscovered ligands. In this manuscript, we show that the TREM2 ectodomain (sTREM2) is monomeric in solution, and since previous structural studies imply that TREM2:DAP12 forms a 1:2

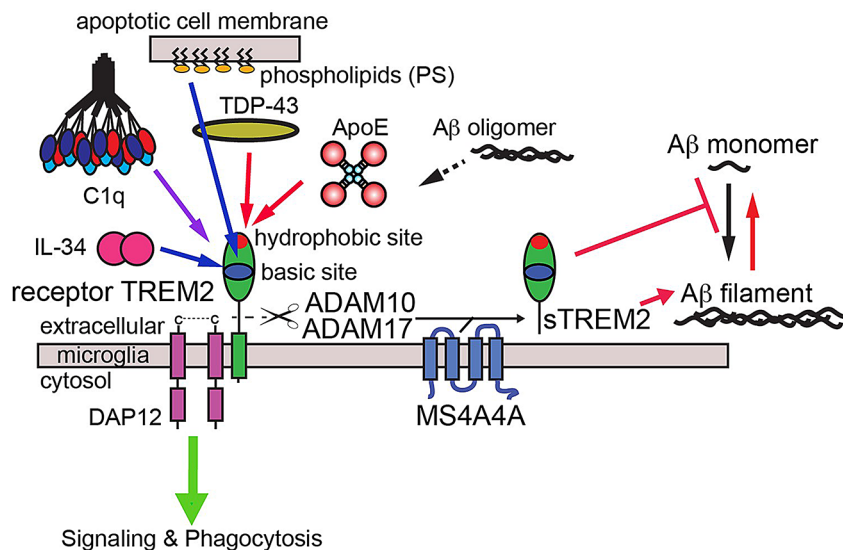


Fig. 10 Graphic schematic for TREM2 interactions with AD ligands. Signaling interactions mapped to the basic site are denoted by blue lines, while signaling interactions mapped to the hydrophobic site are shown as red lines. The binding site for PS is from a previous crystallographic study [22], while the others are comprehensively determined in the current study. Soluble TREM2 (sTREM2) can be produced by proteolytic cleavage [39, 40] or alternative transcripts [41, 42]. Levels of proteolysis produced sTREM2 appear to be modulated by MS4A4A [40]. sTREM2 can inhibit A β polymerization and disaggregate A β filaments [10]

complex (Fig. 10), this would suggest that TREM2 signaling is initiated by oligomeric ligands binding to and clustering TREM2. We have previously shown in highly overexpressed cellular systems that receptor TREM2 might oligomerize, and that this self-association might be disrupted by AD risk variants [38]. Thus these risk variants most likely subtly disrupt clustering after ligand engagement and hence, disrupt downstream signaling. Understanding distinctly how these variants contribute to development of AD will require additional comprehensive structure-function studies to understand how these variants are related to disease, possibly examining interactions in the context of cell membrane and functional output.

Conclusions

Our comprehensive binding studies highlight the surfaces that TREM2 utilizes to engage multiple ligands within the scope of neurodegenerative diseases (Fig. 10). We find that most TREM2 ligands either completely (apoE4 and TDP-43) or partially (C1q) engage the hydrophobic site. In addition, competition binding studies between apoE4 and α A β 42 suggest that α A β 42 also at least partially utilizes the hydrophobic site to engage TREM2. C1q appears to mainly engage the basic site, with some extended contacts in the hydrophobic site. Finally, IL-34 does not appear to engage the hydrophobic site at all, and instead engages a surface on the basic site centered around R76. Previous structural studies have shown that the PS headgroup is mainly recognized by residues in the basic site. Site 2, a site previously identified as a potential

binding site for α A β 42 [8], does not appear to be involved in engaging any of the ligands investigated in this study. These observations suggest that both the hydrophobic and basic sites could be therapeutically targeted to specifically modulate TREM2 interactions with distinct ligands, and therefore modify function and microglia action.

Supplementary Information

The online version contains supplementary material available at <https://doi.org/10.1186/s13024-024-00795-9>.

Supplementary Material 1

Acknowledgements

This work was supported by Alzheimer's Association Research Grant (AARG-16-441560) and Zenith Fellows Award (ZEN-25-1269507)(TJB), Bright Focus Foundation (A2022032S)(TJB), NIH R01HL170198 (TJB and JAB), NIH R01AI159678 and R01AI169850 (DWL), NIH R01HL152245 (JAB), Burroughs Wellcome CAMS 1014685 (JAB), Amgen Scholars Research Fellowships (JAG, JW), and Vagelos Undergraduate Research Fellowship (CZ).

Author contributions

JAG: Study design, obtaining data, data analysis, interpretation of results, writing the manuscript. JRW: obtaining data, data analysis, interpretation of results, revising the manuscript. RAG: obtaining computational data, computational data analysis, interpretation of computational results, writing the manuscript. CZ: obtaining data, data analysis, interpretation of results. DAP and DWL: performing and analyzing SEC-MALS, preparing figures and writing. JS: obtaining data, data analysis, interpretation of results. MW: obtaining data, data analysis, interpretation of results. CC: obtaining data, data analysis, interpretation of results. YS: design of computational study, obtaining computational data, computational data analysis, interpretation of computational results, writing the manuscript. JMA-B: Study design, obtaining data, data analysis, interpretation of results, writing the manuscript. TJB: Obtaining funding, study concept and design, obtaining data, data analysis, interpretation of results, writing the manuscript.

Data availability

Data and materials are available upon request.

Declarations

Ethics approval and consent to participate

N/A.

Competing interests

The authors report no competing interests.

Author details

¹Division of Pulmonary and Critical Care Medicine, Department of Internal Medicine, Washington University School of Medicine, St. Louis, MO, USA

²Department of Biomedical Engineering, University of Alabama, Birmingham, AL, USA

³Division of Infectious Disease, Department of Internal Medicine, Washington University School of Medicine, St. Louis, MO, USA

⁴Center for Regenerative Medicine, Washington University School of Medicine, St. Louis, MO, USA

⁵Department of Pathology and Immunology, Washington University School of Medicine, St. Louis, MO, USA

⁶Department of Biochemistry and Molecular Biophysics, Washington University School of Medicine, St. Louis, MO, USA

⁷Hope Center for Neurological Disorders, Washington University School of Medicine, St. Louis, MO, USA

⁸Department of Cell Biology and Physiology, Washington University School of Medicine, St. Louis, MO 63110, USA

⁹660 S. Euclid, Box 8052, St. Louis, MO 63110, USA

Received: 2 August 2024 / Accepted: 27 December 2024

Published online: 09 January 2025

References

- Deczkowska A, Weiner A, Amit I. The Physiology, Pathology, and potential therapeutic applications of the TREM2 signaling pathway. *Cell*. 2020;181:1207–17.
- Guerreiro R, Wojtas A, Bras J, Carrasquillo M, Rogaeva E, Majounie E, Cruchaga C, Sassi C, Kauwe JS, Younkin S, et al. TREM2 variants in Alzheimer's disease. *N Engl J Med*. 2013;368:117–27.
- Jin SC, Benitez BA, Karch CM, Cooper B, Skorupa T, Carrell D, Norton JB, Hsu S, Harari O, Cai Y, et al. Coding variants in TREM2 increase risk for Alzheimer's disease. *Hum Mol Genet*. 2014;23:5838–46.
- Jonsson T, Stefansson H, Steinberg S, Jonsson I, Jonsson PV, Snaedal J, Bjornsson S, Huttenlocher J, Levey AI, Lah JJ, et al. Variant of TREM2 associated with the risk of Alzheimer's disease. *N Engl J Med*. 2013;368:107–16.
- Shi Q, Gutierrez RA, Bhat MA. Microglia, Trem2, and Neurodegeneration. *Neuroscientist* 2024:10738584241254118.
- Zhong L, Xu Y, Zhuo R, Wang T, Wang K, Huang R, Wang D, Gao Y, Zhu Y, Sheng X, et al. Soluble TREM2 ameliorates pathological phenotypes by modulating microglial functions in an Alzheimer's disease model. *Nat Commun*. 2019;10:1365.
- Ewers M, Franzmeier N, Suarez-Calvet M, Morenas-Rodriguez E, Caballero MAA, Kleinberger G, Piccio L, Cruchaga C, Deming Y, Dichgans M et al. Increased soluble TREM2 in cerebrospinal fluid is associated with reduced cognitive and clinical decline in Alzheimer's disease. *Sci Transl Med* 2019, 11.
- Belsare KD, Wu H, Mondal D, Bond A, Castillo E, Jin J, Jo H, Roush AE, Pilla KB, Sali A et al. Soluble TREM2 inhibits secondary nucleation of Abeta fibrillization and enhances cellular uptake of fibrillar abeta. *Proc Natl Acad Sci U S A* 2022, 119.
- Kober DL, Stuchell-Brereton MD, Kluender CE, Dean HB, Strickland MR, Steinberg DF, Nelson SS, Baban B, Holtzman DM, Frieden C et al. Functional insights from biophysical study of TREM2 interactions with apoE and Abeta(1–42). *Alzheimers Dement* 2020.
- Vilalta A, Zhou Y, Sevalle J, Griffin JK, Satoh K, Allendorf DH, De S, Puigdellicol M, Bruzas A, Burguillos MA, et al. Wild-type sTREM2 blocks abeta aggregation and neurotoxicity, but the Alzheimer's R47H mutant increases abeta aggregation. *J Biol Chem*. 2021;296:100631.
- Atagi Y, Liu CC, Painter MM, Chen XF, Verbeeck C, Zheng H, Li X, Rademakers R, Kang SS, Xu H, et al. Apolipoprotein E is a Ligand for triggering receptor expressed on myeloid cells 2 (TREM2). *J Biol Chem*. 2015;290:26043–50.
- Bailey CC, DeVaux LB, Farzan M. The triggering receptor expressed on myeloid cells 2 binds apolipoprotein E. *J Biol Chem*. 2015;290:26033–42.
- Jendresen C, Arskog V, Daws MR, Nilsson LN. The Alzheimer's disease risk factors apolipoprotein E and TREM2 are linked in a receptor signaling pathway. *J Neuroinflammation*. 2017;14:59.
- Yeh FL, Wang Y, Tom I, Gonzalez LC, Sheng M. TREM2 binds to Apolipoproteins, including APOE and CLU/APOJ, and thereby facilitates uptake of amyloid-Beta by Microglia. *Neuron*. 2016;91:328–40.
- Xie M, Liu YU, Zhao S, Zhang L, Bosco DB, Pang YP, Zhong J, Sheth U, Martens YA, Zhao N, et al. TREM2 interacts with TDP-43 and mediates microglial neuroprotection against TDP-43-related neurodegeneration. *Nat Neurosci*. 2022;25:26–38.
- Neumann M, Sampathu DM, Kwong LK, Truax AC, Micsenyi MC, Chou TT, Bruce J, Schuck T, Grossman M, Clark CM, et al. Ubiquitinated TDP-43 in frontotemporal lobar degeneration and amyotrophic lateral sclerosis. *Science*. 2006;314:130–3.
- Cairns NJ, Neumann M, Bigio EH, Holm IE, Troost D, Hatanpaa KJ, Foong C, White CL 3rd, Schneider JA, Kretschmar HA, et al. TDP-43 in familial and sporadic frontotemporal lobar degeneration with ubiquitin inclusions. *Am J Pathol*. 2007;171:227–40.
- Xie X, Zhang W, Xiao M, Wei T, Qiu Y, Qiu J, Wang H, Qiu Z, Zhang S, Pan Y, et al. TREM2 acts as a receptor for IL-34 to suppress acute myeloid leukemia in mice. *Blood*. 2023;141:3184–98.
- Chhetri G. Emerging roles of IL-34 in neurodegenerative and neurological infectious disease. *Int J Neurosci*. 2023;133:660–71.
- Zhong L, Sheng X, Wang W, Li Y, Zhuo R, Wang K, Zhang L, Hu DD, Hong Y, Chen L, et al. TREM2 receptor protects against complement-mediated synaptic loss by binding to complement C1q during neurodegeneration. *Immunity*. 2023;56:1794–e18081798.
- Kober DL, Alexander-Brett JM, Karch CM, Cruchaga C, Colonna M, Holtzman MJ, Brett TJ. Neurodegenerative disease mutations in TREM2 reveal a functional surface and distinct loss-of-function mechanisms. *Elife* 2016, 5.
- Sudom A, Talreja S, Danao J, Bragg E, Kegel R, Min X, Richardson J, Zhang Z, Sharkov N, Marcora E, et al. Molecular basis for the loss-of-function effects of the Alzheimer's disease-associated R47H variant of the immune receptor TREM2. *J Biol Chem*. 2018;293:12634–46.
- Stine WB Jr., Dahlgren KN, Krafft GA, LaDu MJ. In vitro characterization of conditions for amyloid-beta peptide oligomerization and fibrillogenesis. *J Biol Chem*. 2003;278:11612–22.
- Aricescu AR, Lu W, Jones EY. A time- and cost-efficient system for high-level protein production in mammalian cells. *Acta Crystallogr D Biol Crystallogr*. 2006;62:1243–50.
- Bernhofer M, Dallago C, Karl T, Satagopam V, Heinzinger M, Littmann M, Olenyi T, Qiu J, Schutze K, Yachdav G, et al. PredictProtein - Predicting protein structure and function for 29 years. *Nucleic Acids Res*. 2021;49:W535–40.
- Qiu J, Bernhofer M, Heinzinger M, Kemper S, Norambuena T, Melo F, Rost B. ProNA2020 predicts protein-DNA, protein-RNA, and protein-protein binding proteins and residues from sequence. *J Mol Biol*. 2020;432:2428–43.
- Kyte J, Doolittle RF. A simple method for displaying the hydropathic character of a protein. *J Mol Biol*. 1982;157:105–32.
- Jacchieri SG, Torquato R, Brentani RR. Structural study of binding of flagellin by toll-like receptor 5. *J Bacteriol*. 2003;185:4243–7.
- Dominguez C, Boelens R, Bonvin AM. HADDOCK: a protein-protein docking approach based on biochemical or biophysical information. *J Am Chem Soc*. 2003;125:1731–7.
- Ma X, Lin WY, Chen Y, Stawicki S, Mukhyala K, Wu Y, Martin F, Bazan JF, Starovasnik MA. Structural basis for the dual recognition of helical cytokines IL-34 and CSF-1 by CSF-1R. *Structure*. 2012;20:676–87.
- Greven JA, Brett TJ. Production of eukaryotic glycoproteins for structural and functional studies using Expi293F cells. *Curr Protoc*. 2022;2:e512.
- Lessard CB, Malnik SL, Zhou Y, Ladd TB, Cruz PE, Ran Y, Mahan TE, Chakrabaty P, Holtzman DM, Ulrich JD et al. High-affinity interactions and signal transduction between Abeta oligomers and TREM2. *EMBO Mol Med* 2018, 10.
- Garai K, Verghese PB, Baban B, Holtzman DM, Frieden C. The binding of apolipoprotein E to oligomers and fibrils of amyloid-beta alters the kinetics of amyloid aggregation. *Biochemistry*. 2014;53:6323–31.
- Kober DL, Brett TJ. TREM2-Ligand interactions in Health and Disease. *J Mol Biol*. 2017;429:1607–29.

35. PrabhuDas MR, Baldwin CL, Bollyky PL, Bowdish DME, Drickamer K, Febbraio M, Herz J, Kobzik L, Krieger M, Loike J, et al. A Consensus definitive classification of scavenger receptors and their roles in Health and Disease. *J Immunol*. 2017;198:3775–89.
36. Dean HB, Roberson ED, Song Y. Neurodegenerative Disease-Associated variants in TREM2 destabilize the apical ligand-binding region of the Immunoglobulin Domain. *Front Neurol*. 2019;10:1252.
37. Song W, Hooli B, Mullin K, Jin SC, Cella M, Ulland TK, Wang Y, Tanzi RE, Colonna M. Alzheimer's disease-associated TREM2 variants exhibit either decreased or increased ligand-dependent activation. *Alzheimers Dement*. 2017;13:381–7.
38. Dean HB, Greer RA, Yang SZ, Elston DS, Brett TJ, Roberson ED, Song Y. Multimerization of TREM2 is impaired by Alzheimer's disease-associated variants. *Alzheimers Dement*. 2024;20:6332–50.
39. Feuerbach D, Schindler P, Barske C, Joller S, Beng-Louka E, Worringer KA, Kommineni S, Kaykas A, Ho DJ, Ye C, et al. ADAM17 is the main sheddase for the generation of human triggering receptor expressed in myeloid cells (hTREM2) ectodomain and cleaves TREM2 after histidine 157. *Neurosci Lett*. 2017;660:109–14.
40. Schlepckow K, Kleinberger G, Fukumori A, Feederle R, Lichtenthaler SF, Steiner H, Haass C. An Alzheimer-associated TREM2 variant occurs at the ADAM cleavage site and affects shedding and phagocytic function. *EMBO Mol Med*. 2017;9:1356–65.
41. Del-Aguila JL, Benitez BA, Li Z, Dube U, Mihindukulasuriya KA, Budde JP, Farias FHG, Fernandez MV, Ibanez L, Jiang S, et al. TREM2 brain transcript-specific studies in AD and TREM2 mutation carriers. *Mol Neurodegener*. 2019;14:18.
42. Moutinho M, Coronel I, Tsai AP, Di Prisco GV, Pennington T, Atwood BK, Puntambekar SS, Smith DC, Martinez P, Han S, et al. TREM2 splice isoforms generate soluble TREM2 species that disrupt long-term potentiation. *Genome Med*. 2023;15:11.

Publisher's note

Springer Nature remains neutral with regard to jurisdictional claims in published maps and institutional affiliations.